

A non-covalent “click chemistry” strategy to efficiently coat highly porous MOF nanoparticles with a stable polymeric shell

Ahmet Aykaç,^{a,1} Magali Noiray,^b Milo Malanga,^c Valentina Agostoni,^{b,2} Juan Manuel Casas-Solvas,^a Éva Fenyvesi,^c Ruxandra Gref,^{d,*} Antonio Vargas-Berenguel^{a,*}

^aDepartamento de Química y Física, Universidad de Almería, 04120 Almería, Spain.

^bFaculté de Pharmacie, UMR 8612 CNRS Université Paris-Sud, Châtenay-Malabry, France

^cCycloLab, Cyclodextrin R&D Ltd., Budapest, Hungary

^dISMO, Université Paris Sud, Université Paris Saclay, Orsay, France

¹Present address: Faculty of Engineering and Architecture, Izmir Katip Çelebi University, Çigli, 35620, Izmir, Turkey.

²Present address: Department of Chemistry and Applied Biosciences, Institute of Pharmaceutical Sciences, Eidgenössische Technische Hochschule (ETH), Vladimir-Prelog-Weg 1-5/10 8093 Zürich, Switzerland.

*Corresponding authors at: ISMO, Université Paris Sud, Université Paris Saclay, Orsay, France (R. Gref), Departamento de Química y Física, Universidad de Almería, 04120 Almería, Spain (A. Vargas-Berenguel).

E-mail addresses: ahmet.aykac@ikc.edu.tr (A. Aykaç), magali.noiray@u-psud.fr (Magali Noiray), malanga@cyclolab.hu (M. Malanga), valentina.agostoni@pharma.ethz.ch (V. Agostini), jmcasas@ual.es (J. M. Casas-Solvas), Fenyvesi.e@cyclolab.hu (E. Fenyvesi), ruxandra.gref@u-psud.fr (R. Gref), avargas@ual.es (A. Vargas-Berenguel).

Abstract

Background: Metal-organic framework nanoparticles (nanoMOFs) are biodegradable highly porous materials with a remarkable ability to load therapeutic agents with a wide range of physico-chemical properties. Engineering the nanoMOFs surface may provide nanoparticles with higher stability, controlled release, and targeting abilities. Designing postsynthetic, non-covalent self-assembling shells for nanoMOFs is especially appealing due to their simplicity, versatility, absence of toxic byproducts and minimum impact on the original host-guest ability.

Methods: In this study, several β -cyclodextrin-based monomers and polymers appended with mannose or rhodamine were randomly phosphorylated, and tested as self-assembling coating building blocks for iron trimesate MIL-100(Fe) nanoMOFs. The shell formation and stability were studied by isothermal titration calorimetry (ITC), spectrofluorometry and confocal imaging. The effect of the coating on tritium-labelled AZT-PT drug release was estimated by scintillation counting.

Results: Shell formation was conveniently achieved by soaking the nanoparticles in self-assembling agent aqueous solutions. The grafted phosphate moieties enabled a firm anchorage of the coating to the nanoMOFs. Coating stability was directly related to the density of grafted phosphate groups, and did not alter nanoMOFs morphology or drug release kinetics.

Conclusion: An easy, fast and reproducible non-covalent functionalization of MIL-100(Fe) nanoMOFs surface based on the interaction between phosphate groups appended to β -cyclodextrin derivatives and iron(III) atoms is presented.

General Significance: This study proved that discrete and polymeric phosphate β -cyclodextrin derivatives can conform non-covalent shells on iron(III)-based nanoMOFs. The flexibility of the β -cyclodextrin to be decorated with different motifs open the way towards nanoMOFs modifications for drug delivery, catalysis, separation, imaging and sensing.

Keywords

MIL-100(Fe) nanoMOFs, β -cyclodextrin, phosphorylation, non-covalent coating, AZT-TP

Abbreviations

MOF: Metal-organic framework; β -CD: β -cyclodextrin; NMR: nuclear magnetic resonance; DLC: dynamic light scattering; TEM: transmission electron microscopy; ITC: isothermal titration calorimetry; CD-P: β -cyclodextrin phosphate sodium salt; CD-P-M: mannosylated β -cyclodextrin phosphate sodium salt; CD-P-R: rhodamine- β -cyclodextrin phosphate sodium

salt; EP: epichlorohydrin; polyCD: epichlorohydrin-crosslinked β -CD polymer; MIL-100(Fe): Material from Institute Lavoisier, iron trimesate nanoMOFs; AZT-TP: 3'-azidothymidine triphosphate.

1. Introduction

The use of nanotechnology for drug delivery applications is changing the landscape of pharmaceutical and biotechnology industries opening new opportunities for more efficient and personalized treatments. Among the large variety of nanomaterials explored for this purpose, metal-organic frameworks (MOFs) [1] keep attracting a growing interest due to their useful applications in gas storage, separation, catalysis, sensing, etc. [2,3,4] and, more recently, in biomedicine. [3,4,5,6,7,8,9,10,11] Some of the key advantages of MOFs are their easily tunable and versatile composition, as well as their large variety in terms of pore sizes and shapes. In particular, nanosized MOFs (nanoMOFs) based on porous iron(III) polycarboxylates emerged as a new class of biodegradable and non-toxic nanomaterials [12]. Various challenging therapeutic molecules could be entrapped within the interconnected porous structure reaching unprecedented loadings (within the 20-70 wt % range). In addition, a controlled release in simulated body fluid was achieved, while the iron(III) nanoMOFs exhibited high relaxivities making these particles interesting candidates for teranostics [5].

The use of nanomaterials in biomedicine has risen new challenging goals such as: (i) targeted drug delivery; (ii) bypassing across biological barriers; (iii) delivery of drugs to intracellular targets and (iv) imaging of sites of drug delivery. To address these challenges, the use of nanoparticles with engineered shells is mandatory since the *in vivo* fate of nanoparticles (biodistribution, pharmacokinetics and targeting abilities) is intimately related to their surface physicochemical properties [13,14]. Engineered core-shell nanoparticles should be able not only contain high drug payloads (preferably, > 20wt%) and release the drugs in a controlled fashion, but they should be also easily coated through a "green" versatile process without altering neither the drug payloads nor the drug integrity. Besides, the coating shell should be stable enough in biological media to exert its therapeutic activity.

Coating preformed nanoparticles with a stable, covalent coating often involves several time consuming reaction steps and generates side products difficult to be totally removed. Traces of these side products and/or organic solvents might raise toxicological concerns in view of clinical applications. Moreover, during the coating process drugs can leak out or lose their activity. One trend for coating strategies relies on "click chemistry", and more specifically on the copper-catalyzed azide-alkyne cycloaddition reaction, in reason of its rapidity and possibility of being carried out in aqueous media [15,16,17,18]. However, yields are not always high, especially in the case of bulky molecules due to the formation of alkyne homocoupling side products, among other reasons.

As a strategy to overcome these drawbacks, we have recently reported a non-covalent procedure enabling to coat, practically instantaneously, preformed MIL-100(Fe) (MIL standing for Material from Institute Lavoisier) nanoMOFs, built up from iron(III) octahedral trimers and trimesate linkers (1,3,5-benzene tricarboxylate), with phosphate-decorated cyclooligosaccharide β -cyclodextrin (β -CD) shell (Fig. 1) [19]. The coating was achieved directly in water following a “green” method which does not involve organic solvents, nor produces side products. This strategy took advantage of the ability of polar phosphate groups to coordinatively bind the unsaturated metallic Lewis acid sites on the nanoMOFs surface, forming a stable shell.

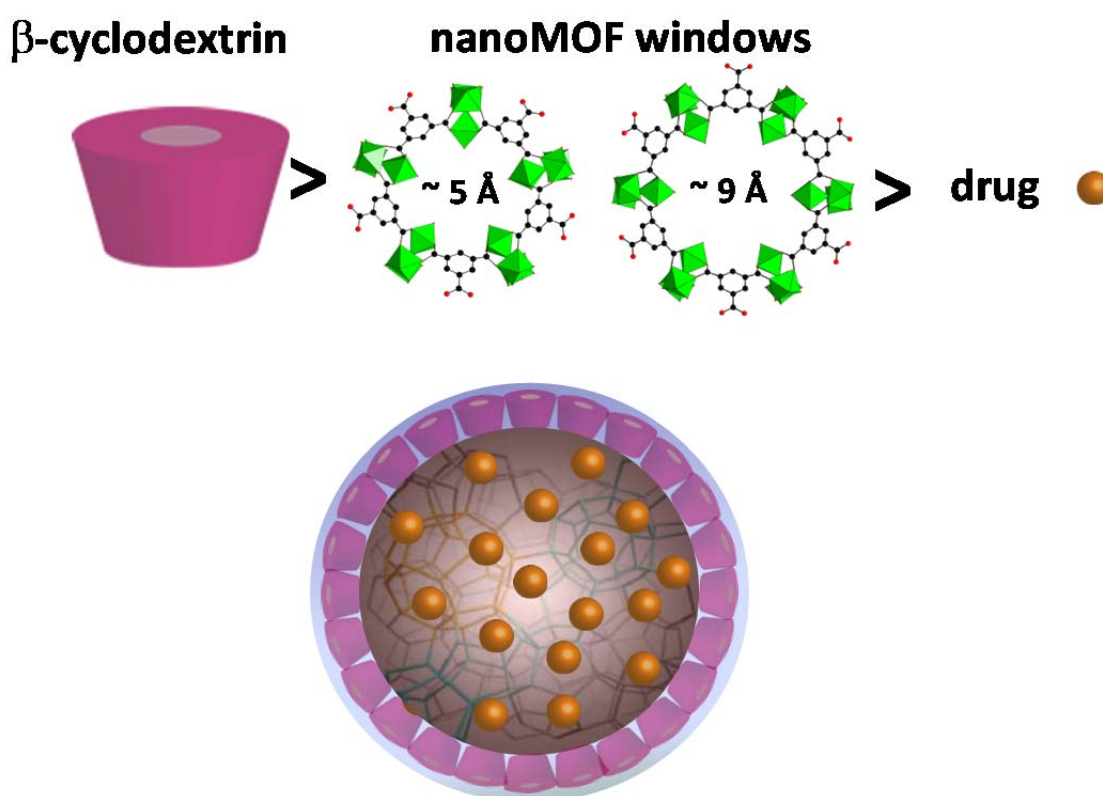


Fig. 1. Schematic representation of a porous nanoMOF particle entrapping a drug and coated with a CD-based shell. Bulky CD molecules (pink) are too large to cross the pentagonal and the hexagonal nanoMOF windows so they cannot get adsorbed within the nanoMOF porous inner structure. On the contrary, drug molecules (yellow) penetrate within the open porous structure filling the nanoMOFs pores.

β -CD is a naturally occurring cyclic oligosaccharide comprising seven D-glucopyranose units linked by α -(1 \rightarrow 4) bonds. This biocompatible macrocycle possesses a relatively rigid torus-shaped structure, which defines an inner hydrophobic cavity rimmed by two hydrophilic openings. β -CD is well-known to form inclusion complexes in aqueous solution with a large variety of organic molecules of hydrophobic nature and suitable size and geometry [20,21,22] and it is a suitable scaffold for introducing functional groups for targeting and

imaging purposes [23]. Due to its ability to improve the physicochemical properties of drugs (stability, solubility and bioavailability) [22] CDs are considered as “smart” components when incorporated in drug delivery devices [24].

In view of these properties, the modification of nanoMOFs cores with β -CD-based shells appears as particularly appealing. This association is feasible due to the fact that β -CD outer diameter is 15.4 Å, the average value for its radii of the hydrodynamic equivalent sphere being 7.7 Å [25]. In contrast, MIL-100(Fe) nanoMOFs shows a porous architecture delimiting large (29 Å) and small (24 Å) mesoporous cages which are accessible through microporous pentagonal (5.6 Å) or hexagonal windows (8.6 Å) [26]. Thus, bulky CD molecules cannot penetrate the nanoMOF tridimensional core structures (Fig.1).

Water soluble β -CD polymers remarkably increase the solubility of hydrophobic drugs as compared to their monomers (β -CDs) [27,28,29]. In addition, polymeric CD shells have some advantages over the monomeric ones, such as the obtention of thicker coatings, which in turn may lead to increased stability, better control of drug release and facilitated shell functionalization with fluorescent dyes or targeting ligands. However, ensuring stable thick polymeric shells on porous MOFs, without using any organic solvent or coupling agent, is not a trivial issue. Indeed, shell stability is related to the density and accessibility of the anchoring moieties. While a high effective concentration of interacting appendages is expected in the case of persubstituted discrete β -CD derivatives resulting in a multivalent effect, additional factors may be involved in the case of β -CD polymers, including higher steric hindrance, different spatial distribution of the anchors depending on the derivatisation degree, induce-fit effects or possibility of cross-linking between several nanoparticles. As a result, it is difficult to predict the behaviour of a given β -CD polymer as a coating shell on MOFs nanoparticles.

Despite these interesting features, the use of CD polymers to coat nanoMOFs has not been explored yet. In order to shed some light on this challenging goal, this work describes the synthesis of several phosphorylated discrete and polymeric β -CD derivatives, some of them containing functional moieties such as mannose and rhodamine. The surface functionalization of MIL-100(Fe) nanoMOFs with these compounds, drug entrapment and the characterization of the hybrid nanoassemblies are studied and compared using complementary techniques.

2. Materials and methods

2.1. Materials

Thin layer chromatography (TLC) was performed on Merck silica gel 60 F254 aluminum sheets and developed by UV-vis light and ethanolic sulfuric acid (5% v/v). Flash column chromatography was performed on Merck silica gel (230–400 mesh, ASTM). Melting points

were measured on a Büchi B-450 melting point apparatus and are uncorrected. Optical rotations were recorded on a Jasco P-1030 polarimeter at room temperature. $[\alpha]_D$ values are given in $10^{-1} \text{ deg cm}^{-1} \text{ g}^{-1}$. Infrared spectra were recorded on a Bruker Alpha FTIR equipped with a Bruker universal ATR sampling accessory. ^1H , ^{13}C and ^{31}P NMR spectra were recorded on a Varian VXR-600 spectrometer, a Bruker Avance DPX300 spectrometer equipped with a QNP $^1\text{H}/^{13}\text{C}/^{19}\text{F}/^{31}\text{P}$ probe, or a Bruker Avance 500 Ultrashield spectrometer equipped with an inverse TBI $^1\text{H}/^{31}\text{P}/\text{BB}$ probe, depending on the sample. Standard Varian and Bruker software was used for acquisition and processing routines. Chemical shifts (δ) are given in parts per million (ppm) and referenced to internal tetramethylsilane (TMS) signal (δ_{H} , δ_{C} 0.00). J values are given in hertz (Hz). MALDI-TOF mass spectra were recorded on a 4800 Plus AB SCIEX spectrometer with 2,5-dihydroxybenzoic acid (DHB) as the matrix. ESI-TOF mass spectra were measured on a Waters Xevo Qtof spectrometer. ICP-OES results were obtained by using a Thermo Scientific iCAP 6500 DUO inductively coupled plasma optical emission spectrophotometer. All aqueous procedures used pure water (Milli-Q, 18.2 M Ω cm) obtained from a Millipore Milli-Q Plus system (Millipore SpA, Milan, Italy). Water, 0.01 M Tris buffer at pH 7.4, or 9.5 mM phosphate buffer saline (Dulbecco's phosphate buffer saline without calcium and magnesium, Lonza) were used as solvents or dispersing media. Dialysis was performed in Milli-Q water using 3.500 kDa molecular weight cutoff (MWCO) membranes (Spectra/Por, regenerated cellulose). Dynamic light scattering (DLS) measurements were performed on a Malvern Zetasizer Nano-ZS analyzer. Transmission electron microscopy (TEM) analyses were carried out on a Darwin 208 Philips microscope (60-80-100 KV; Camera AMT). Spectrofluorimetry measurements were recorded on a Perkin Elmer Luminescence LS50B spectrometer.

Cooper (II) sulfate anhydrous ($\geq 98\%$, Fluka), sodium L-ascorbate ($\geq 98\%$, Sigma-Aldrich), β -CD (99%, Roquette), β -CD phosphate sodium salt (CD-P, Cyclolab, DS 2-6), iron(III) chloride hexahydrate (98%, Alfa Aesar), 1,3,5-benzenetricarboxylic acid (1,3,5-BTC, 95 %, Aldrich), epichlorohydrin (EP, 99%, Aldrich), phosphorus pentoxide (99%, Aldrich), absolute ethanol (99%, Carlo Erba), 3'-azidothymidine triphosphate (AZT-TP, 3'-azido-2',3'-dideoxythymidine-5'-triphosphate lithium salt, TriLink) and radioactive AZT-TP-methyl [^3H] (azido 3'-deoxythymidine 5'-triphosphate, tetratriethylammonium salt [methyl- ^3H], Movarek) were purchased from described commercial sources and used without further purification otherwise indicated. B-CD was dried at 50 °C in vacuum in the presence of P_2O_5 until a constant weight was achieved. Organic solvents were dried according to literature procedures [30].

2.2 Synthesis of mannosylated and rhodamine-containing β -CD phosphate sodium salts CD-P-M **4** and CD-P-R **6**.

Synthesis of 2'-O-[1-(2,3,4,6-tetra-O-acetyl- α -D-mannopyranosiloxyethyl)-1H-1,2,3-triazol-4-ylmethyl]cyclomaltoheptaose (**3**): To a stirred solution of 2-azidoethyl 2,3,4,6-tetra-O-acetyl- α -D-mannopyranoside **2** [31] (62 mg, 0.148 mmol) in THF (4 mL) was added 2'-O-propargyl

cyclomaltoheptaose **1** [32,33] (174 mg, 0.148 mmol), followed by CuSO₄ (4.3 mg, 0.029 mmol) and a solution of sodium L-ascorbate (15 mg, 0.074 mmol) in water (4 mL). The reaction mixture was stirred at room temperature for 18 h and the solvent was evaporated at reduced pressure. The crude product was purified by column chromatography using CH₃CN-H₂O-(30% v/v aq NH₃) 10:5:1 as eluent to yield compound **3** (142.2 mg, 76 %) as a white solid. Mp 213°-215 °C (dec.); [α]_D +112.3° (c 0.2, H₂O); IR (KBr): 3390, 2941, 2117, 1750, 1646, 1156, 1081, 1029 cm⁻¹; ¹H NMR (300 MHz, D₂O): δ 8.10-8.20 (bs, 1H, triazol-H), 4.97-5.09 (m, 3H, H-2',3',4'), 4.96 (s, 1H, H-1'), 4.60-4.84 (bs, 6H, H-1), 3.50-3.75 (m, 34H, H-3,5,6), 3.30-3.50 (m, 18H, H-2,4), 1.80-2.01 (s, 12H, CH₃CO); ¹³C NMR (75 MHz, D₂O): δ 170.1, 169.7, 143.7, 102.0, 96.4, 81.7, 73.2, 72.8, 72.5, 72.1, 71.9, 68.6, 68.0, 65.8, 65.2, 60.0, 49.0, 22.7, 20.6, 20.5, 20.4; ESI-TOF-MS *m/z* calcd for C₆₁H₉₅N₃O₄₅ 1590.4, found 1590.4 [M + Na]⁺.

Synthesis of 2¹-O-[1- α -D-mannopyranosiloxyethyl)-1H-1,2,3-triazol-4-ylmethyl]cyclomaltoheptaose phosphate sodium salt (CD-P-M, **4**): P₂O₅ (200 mg, 1.4 mmol) was added to dried DMF (3 mL) and the mixture was ultrasonicated in a tightly-closed flask until obtaining a clear solution. Compound **3** (80 mg, 0.053 mmol) was added to the solution and the reaction mixture was stirred for 18 h at 40 °C. Then, the pH was set to 12 using 1 M NaOH and the mixture was stirred for 18 h at room temperature. The solution was neutralized (pH ~7) with 5 M HCl and stirred at room temperature for 1 h, dialyzed against water for 5 days and freeze-dried to yield CD-P-M **4** as a white solid (143.3 mg, 71%). Mp 224-226 °C (dec.); [α]_D +118.6° (c 0.2, H₂O); IR (KBr): 3150, 1653, 1504, 1437, 1348 (P=O), 921, 685, cm⁻¹; ¹H NMR (300 MHz, D₂O): δ 8.01 (s, 1H, triazol-H), 5.25 (s, 1H), 4.92-4.98 (m, 10H), 4.73-4.76 (bs, 7H), 3.69-3.80 (m, 28H), 3.43-3.51 (m, 18H); ¹³C NMR (75 MHz, D₂O): δ 170.9, 170.4, 144.5, 125.5, 102.8, 96.7, 82.4, 73.9, 73.5, 73.2, 72.9, 72.6, 71.9, 69.3, 68.7, 66.6, 66.0, 62.5, 60.8, 49.8; ³¹P NMR (121.5 MHz, D₂O): δ 1.7, 1.2, -8.1, -9.0, -9.7, -9.8, -10.0, -20.9. ICP-OES: Calc. for C₅₃H₆₇N₃Na₂₀O₁₀₁P₂₀ (3441.3): P, 18.0%. Found: P 18.0%

Synthesis of 6-monodeoxy-6-mono[(5/6)-rhodaminythioureido]- β -CD phosphate sodium salt (CD-P-R, **6**): P₂O₅ (200 mg, 1.4 mmol) was added to dried DMF (3 mL) and the mixture was ultrasonicated in a tightly-closed flask until obtaining a clear solution. Then, 6-monodeoxy-6-mono[(5/6)-rhodaminythioureido]- β -CD hydrochloride **5** (mixture of regioisomers) [34] (235 mg, 0.14 mmol) was added and the reaction mixture was stirred at 40 °C for 4 h. Temperature was then allowed to cool down, water (20 mL) was added and the obtained solution was dialyzed for 1 day. The solution was neutralized (pH ~7) with 1 M NaOH and dialyzed for 1 day. The pH of the solution was adjusted to 7-8 with 1 M NaOH and then washed with water-saturated ethyl acetate (4x30 mL). Water was removed under reduced pressure at 60 °C till dryness, and the obtained solid was dissolved in water (20 mL), dialyzed overnight and then freeze-dried to yield CD-P-R **6** as a violet powder (229 mg, 84%). Mp: 229-232 °C (dec.); IR (KBr): 3390, 1647, 1594, 1467, 1414, 1348 (P=O), 921, 685, 517 cm⁻¹; ³¹P NMR (121.50 MHz, D₂O): δ 2.3-1.2, -2.8, -3.0, -10.8, -11.3, -21.5, -21.8.

2.3 Synthesis of phosphate β -CD polymers **9a-c** and **10a,b**.

Epichlorohydrin-crosslinked β -CD polymer (polyCD) **7** was synthesized by modifying a previously published procedure [35,36]. Briefly, anhydrous β -CD (100 g) was dissolved in 33% w/w NaOH (160 mL) under mechanical stirring. Then, EP (81.52 g) was rapidly added and the solution was heated to 30 °C. The reaction was stopped in the vicinity of the gelation point by addition of acetone. The obtained reaction mixture phase was heated at 50 °C overnight and neutralized with 6 N HCl to pH 7. PolyCD was finally recovered by freeze-drying. The β -CD content, as determined by ^1H NMR spectroscopy, was 60 % w/w and the average molar mass was 2×10^4 g/mol, as determined by gel permeation chromatography. The synthesis of rhodamine-labeled analogue polyCD-R **8** was achieved as previously reported [37].

Synthesis of polyCD phosphate sodium salt polyCD-P_{1:10} **9a** (molar ratio phosphorus atom-CD unit 1:10): P₂O₅ (12 mg, 0.08 mmol) was added to dried DMF (5 mL) and the mixture was ultrasonicated in a tightly-closed flask until obtaining a clear solution. PolyCD **7** (300 mg, estimated CD content 0.18 g, \sim 0.16 mmol) was added to the solution and the reaction mixture was stirred at 40 °C for 6 h. After cooling to room temperature, water (10 mL) was added and the solution was neutralized (pH \sim 7) with 1 M NaOH and dialyzed against water for 2 days (cut-off membrane 500-1000 Dalton). The solution was centrifuged, and the supernatant was dialyzed again overnight and then freeze-dried to yield polyCD-P_{1:10} **9a** (280 mg) as a white powder.

Synthesis of polyCD phosphate sodium salt polyCD-P_{1:1} **9b** (molar ratio phosphorus atom-CD unit 1:1): P₂O₅ (120 mg, 0.8 mmol) was added to dried DMF (5 mL) and the mixture was ultrasonicated in a tightly-closed flask until obtaining a clear solution. PolyCD **7** (300 mg, estimated CD content 0.18 g, \sim 0.16 mmol) was added to the solution and the reaction mixture was stirred at 40 °C for 6 h. After cooling to room temperature, water (10 mL) was added and the solution was neutralized (pH \sim 7) with 1 M NaOH and dialyzed against water for 2 days (cut-off membrane 500-1000 Dalton). The solution was centrifuged, and the supernatant was dialyzed again overnight and then freeze-dried to yield polyCD-P_{1:1} **9b** (330 mg) as a white powder.

Synthesis of polyCD phosphate sodium salt polyCD-P_{1:5} **9c** (molar ratio phosphorus atom-CD unit 1:5): P₂O₅ (24 mg, 0.16 mmol) was added to dried DMF (5 mL) and the mixture was ultrasonicated in a tightly-closed flask until obtaining a clear solution. PolyCD **7** (300 mg, estimated CD content 0.18 g, \sim 0.16 mmol) was added to the solution and the reaction mixture was stirred at 40 °C for 6 h. After cooling to room temperature, water (10 mL) was added and the solution was neutralized (pH \sim 7) with 1 M NaOH and dialyzed against water for 2 days (cut-off membrane 500-1000 Dalton). The solution was centrifuged, and the supernatant was dialyzed again overnight and then freeze-dried to yield polyCD-P_{1:5} **9c** (300 mg) as a white powder.

Synthesis of rhodamine-labeled polyCD phosphate sodium polyCD-P_{1:10}-R **10a** (molar ratio phosphorus atom-CD unit 1:10): P₂O₅ (12 mg, 0.08 mmol) was added to dried DMF (5 mL)

and the mixture was ultrasonicated in a tightly-closed flask until obtaining a clear solution. PolyCD-R **8** (300 mg, estimated CD content 0.18 g, ~0.16 mmol) was added to the solution and the reaction mixture was stirred at 40 °C for 6 h. After cooling to room temperature, water (10 mL) was added and the solution was neutralized (pH ~7) with 1 M NaOH and dialyzed against water for 2 days (cut-off membrane 500-1000 Dalton). The solution was centrifuged, and the supernatant was dialyzed again overnight and then freeze-dried to yield polyCD-P_{1:5} **10a** (250 mg) as a pink powder.

Synthesis of rhodamine-labeled polyCD phosphate sodium salt polyCD-P_{1:1}-R **10b** (molar ratio phosphorus atom-CD unit 1:1): P₂O₅ (120 mg, 0.8 mmol) was added to dried DMF (5 mL) and the mixture was ultrasonicated in a tightly-closed flask until obtaining a clear solution. PolyCD-R **8** (300 mg, estimated CD content 0.18 g, ~0.16 mmol) was added to the solution and the reaction mixture was stirred at 40 °C for 6 h. After cooling to room temperature, water (10 mL) was added and the solution was neutralized (pH ~7) with 1 M NaOH and dialyzed against water for 2 days (cut-off membrane 500-1000 Dalton). The solution was centrifuged, and the supernatant was dialyzed again overnight and then freeze-dried to yield polyCD-P_{1:5} **10c** (290 mg) as a pink powder.

2.4 MIL-100(Fe) iron-carboxylate nanoMOFs synthesis and characterization

MIL-100(Fe) iron-carboxylate nanoMOFs was synthesized by microwave assisted hydrothermal reaction as previously described [38]. Briefly, a mixture of iron(III) chloride hexahydrate (6.0 mmol) and 1,3,5-benzenetricarboxylic acid (4.02 mmol) in deionized water (20 mL) was heated at 130 °C for 6 min under stirring. The power applied was 400 Watt (Mars-5, CEM, US: Power maximum output 1600 ± 240 Watts, frequency at full power 2450 MHz). The as-synthesized nanoparticles were recovered by centrifugation (10 min at 10000 g). Residual non reacted organic acid were removed by washing with absolute ethanol (50 mL) and centrifugation (10 min at 10000 g). This purification step was repeated 6 times.

Crystallinity and purity of MIL-100(Fe) nanoMOFs were assessed by X-ray powder diffraction (XRPD). Patterns were collected in a high resolution D5000 Bruker diffractometer ($\lambda_{\text{Cu}} \text{K}\alpha_1, \text{K}\alpha_2$) from 3° to 20° (2 θ) using a step size of 0.02° and 4° per step in continuous mode. The nanoparticles porous surface was measured by nitrogen sorption experiments at 196°C on an ASAP 2020 (Micromeritics) after sample's outgassing at 100°C for 18 h under secondary vacuum (< 10⁻⁶ Torr). The nanoMOF size and morphology were characterized by dynamic light scattering (DLS) and TEM, respectively.

The nanoparticles were stored in ethanol at room temperature and further used for *in vitro* assays.

2.5 MIL-100(Fe) nanoMOFs surface modification with different coating molecules

MIL-100(Fe) nanoMOFs (2 mg) were modified by impregnation with CD-P, CD-P-M **4**, CD-P-R **6**, polyCD-P_{1:10} **9a**, polyCD-P_{1:1} **9b**, polyCD-P_{1:10}-R **10a**, or polyCD-P_{1:1}-R **10b** aqueous solutions

(2 mg mL⁻¹, 500 μL) under rotative agitation for 1 h at room temperature in the dark. After incubation nanoMOFs were recovered by centrifugation (10 min at 10000 g) and washed twice with water to remove the excess of coating molecules not associated to the nanoparticles surface. For fluorescent rhodamine-containing coating molecules, supernatants were collected, combined and analyzed by emission spectrofluorimetry ($\lambda_{\text{ex}} = 556 \text{ nm}$, $\lambda_{\text{em}} = 576 \text{ nm}$) in order to assess the concentration of the free CD derivatives. The amount of coating molecules associated (coating wt%) to the MIL-100(Fe) nanoMOFs surface was defined by difference as indicated in equation 1:

$$\text{Coating (wt\%)} = \frac{\text{CD derivative (mg)}}{\text{CD derivative (mg)} + \text{MIL-100(Fe) (mg)}} \quad (1)$$

2.6 Shell stability for MIL-100(Fe) nanoMOFs coated with rhodamine-containing β -CD derivatives CD-P-R **6** and polyCD-P-Rs **10a,b**.

MIL-100(Fe) nanoMOFs coated with CD-P-R **6** or polyCD-P-Rs **10a,b**. (1 mg) were incubated in 9.5 mM PBS (1 mL) at pH 7.4 under rotative agitation in the dark at 37 °C. After different time lapses (0.5, 2.5, 5 and 24 h) the mixture was centrifugated (10 min at 9500 g), and 0.5 mL of supernatant was removed and subsequently replaced with the same volume of fresh buffer. Concentration of released CD-P-R or polyCD-P-Rs in the supernatant was quantified by spectrofluorimetry ($\lambda_{\text{ex}} = 556 \text{ nm}$, $\lambda_{\text{em}} = 576 \text{ nm}$).

MIL-100(Fe) nanoMOFs coated with CD-P-R **6** were incubated in RPMI supplemented with 10% fetal bovine serum FBS for 24 h at 37 °C in the dark. Confocal images before and after incubation were recorded on an inverted confocal laser scanning microscope LSM 510-Meta (Carl Zeiss, Germany) using a Plan-Apochromat 63X/1.4 objective lens, equipped with an argon (488 nm excitation wavelength) and a helium neon laser (543 nm excitation wavelength). Rhodamine fluorescence was collected with a 560 nm long pass emission filter under a sequential mode. The pinhole was set at 1.0 Airy unit. 12 bit numerical images were acquired with LSM 510 software version 3.2.

2.7 ITC experiments

An isothermal calorimeter (VP-ITC, MicroCal, GE Healthcare Life Sciences) was used to evaluate the interactions between MIL-100(Fe) nanoMOFs and the different CD derivatives under investigation. The ITC instrument was calibrated electrically using an internal electric heater, and chemically by measuring the dilution enthalpy of methanol in water. This standard reaction was in excellent agreement (1-2 %) with MicroCal constructor data. In a typical experiment, aliquots of 10 μL of CD derivatives (2 to 5 mM) aqueous solutions (283 μL) were injected into a suspension of MIL-100(Fe) (1 or 2 mM; these concentrations are referred to the iron trimers defined by the previously calculated molecular formula [5,39]) in the calorimetric cell (1.441 mL) accurately thermostated at 25 °C. Intervals between injections were 500 s and agitation speed was 268 rpm. For CD-P-M **4**, a slightly different procedure was used to visualize the heat flow: the 10 first injections of 2 μL were followed

by 10 injections of 5 μL and the last ones of 10 μL . In addition, the stirring speed was increased to 806 rpm. Background of titration consisted on injecting the CD derivatives aqueous solutions in solely MilliQ water placed in the sample cell. The corresponding heat flow recorded as a function of time accounts for dilution effect.

2.8 AZT-TP release from modified MIL-100(Fe) nanoMOF

MIL-100(Fe) nanoMOFs were loaded with a tritium-labelled azidothymidine triphosphate (AZT-TP) aqueous solution, as previously described [5,39]. Nanoparticles (2.5 mg) were incubated with 400 $\mu\text{g}/\text{mL}$ AZT-TP aqueous solution (500 μL) marked with 1% of AZT-TP [^3H] (50 $\mu\text{L}/3\text{mL}$, 3.8 Ci/mmol) for 24 h under rotative agitation at room temperature. Subsequently nanoparticles were recovered by centrifugation (10 min at 10000 g). The radioactivity present in the supernatant was determined by scintillation counting using a Beckman Coulter apparatus (LS 6500 multi-purpose scintillation counter) and the drug payload was determined by difference. The drug payloads (AZT-TP wt%) were calculated according to equation 2:

$$\text{AZT-TP payload wt\%} = \frac{\text{AZT-TP (mg)}}{\text{MIL-100(Fe) (mg)}} \% \quad (2)$$

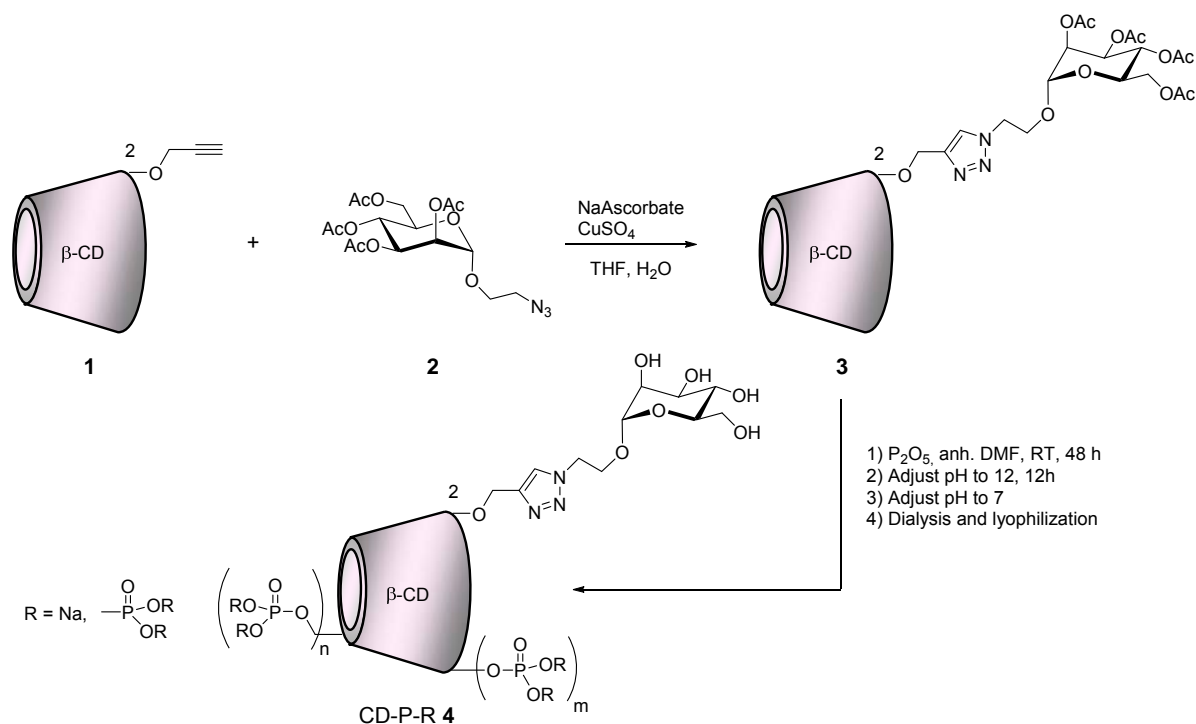
As-prepared AZT-TP loaded MIL-100 nanoMOFs (2.5 mg) were incubated for 1 h under rotative stirring at room temperature with 2.5 mg mL^{-1} CD-P aqueous solution (500 μL), 2.5 mg mL^{-1} polyCD-P_{1:10} **9a** or polyCD-P_{1:5} **9c** aqueous solution (500 μL), or water (500 μL) as control. After incubation the nanoparticles were recovered by centrifugation (10 min at 10000 g). The supernatant was analyzed by scintillation counting to determine the drug released during surface modification. Finally, the nanoparticles were incubated in PBS (1 mL) at 37 °C under rotative stirring. After different incubation times (0.5, 2.5, 5, 8, 24 h), the mixture was centrifugated (10 min at 10000g), 500 μL of supernatant were removed and replaced with the same amount of fresh medium. The collected supernatants were analyzed by scintillation counting in order to evaluate the AZT-TP release from unmodified, CD-P- or polyCD-P modified MIL100(Fe) nanoMOFs.

3. Results and discussion

3.1 Synthesis of CD phosphate derivatives.

Recently we have demonstrated that phosphorylated β -CD (CD-P) can firmly anchor on iron-based MOFs surface forming a non-covalent shell that makes the nanoparticles biocompatible and enhances their stability in water [19]. Interestingly, β -CD is a very flexible scaffold that can be decorated with different appendages, even simultaneously. In this regard, mono-2-*O*-propargyl- β -CD **1** (Scheme 1) is a very convenient building block for the synthesis of β -CD derivatives functionalized on the secondary face. It contains a terminal alkyne group linked to the macrocycle at only one of the seven O-2 positions, which offers the possibility of coupling functional structures by using Cu(I)-catalyzed alkyne-azide cycloaddition while the rest of OH groups remain available [32,33]. Such feature would allow

us to design β -CD-based coating building blocks for iron MOF nanoparticles containing different motifs linked to the secondary face of the cyclooligosaccharide. In order to proof this concept, we designed a randomly phosphorylated β -CD derivative (**4**) containing a mannose moiety that potentially may serve as site-specific delivery vector. Indeed, mono- and disaccharides are very often used to provide nanostructures with bio-specificity [18,23].

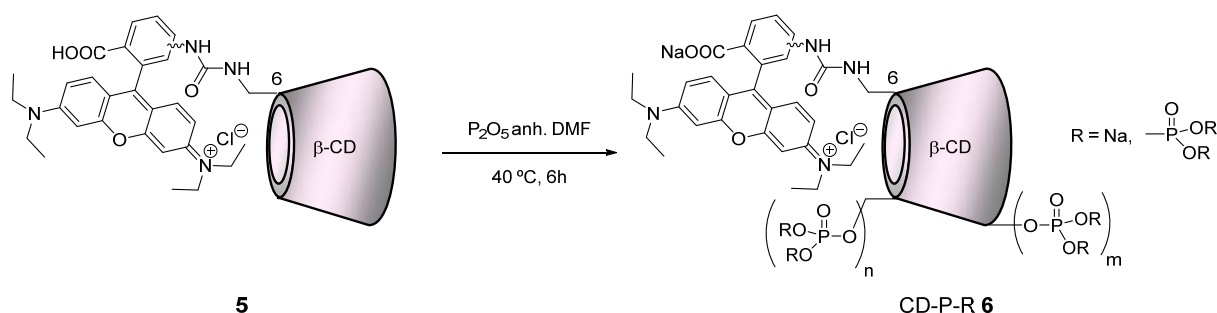


Scheme 1. Synthesis of mannosylated β -CD phosphate sodium salt CD-P-M **4**. Phosphorylation is a random process that can take place at any hydroxylated position and may introduce both phosphate and oligophosphate groups.

The synthesis of such building block is outlined in Scheme 1. The reaction of alkyne- β -CD **1** with peracetylated 2-azidoethyl α -D-mannopyranoside **2** in the presence of sodium ascorbate and CuSO_2 afforded mannosylated β -CD **3** in 76% yields after column chromatography purification. The molecular weight of **3** was verified by MALDI-TOF mass spectrometry. We used NMR spectroscopic techniques with COSY, HMQC, and HMBC experiments for its characterization. ^1H NMR spectrum showed the absence of a signal at 3.52 ppm, corresponding to the alkyne proton in compound **1**, and the appearance of a signal at 8.15 ppm corresponding to the triazol proton. In the ^{13}C NMR spectrum a series of peaks between 170.4 and 170.0 ppm appeared indicating the presence of acetyl groups, as well as one set of signals at 102.3 ppm and a peak at 96.7 ppm assigned to the anomeric carbons of the β -CD and the mannose moieties, respectively. Likewise, alkyne carbons signals observed at 79.9 and 77.8 ppm on the spectrum of **1** did not appear on the spectrum of **3**. Instead, the latter showed peaks at 144.1 and 125.0 ppm corresponding to triazol C-4 and C-5 carbons, respectively. Random phosphorylation of compound **3** was carried out by

treatment with a DMF solution containing an excess of P_2O_5 for 18 h at 40 °C [40,41]. Subsequently, pH of the resulting mixture was increased to 12 by adding an aqueous solution of NaOH in order to remove the acetyl groups. Thereafter, the reaction mixture was neutralized with aqueous HCl and dialyzed for 5 days giving rise to CD-P-M **4** after removing the solvent by lyophilization. Both 1H NMR and ^{13}C NMR spectra of CD-P-M **4** did not show signals assignable to acetyl groups, confirming their removal from the mannoside moiety. ^{31}P NMR spectra showed several peaks in the range from 1.7 to -20.9 ppm attributable to the resonance of the phosphorous nuclei present on the macrocycle. The estimated value for the content of phosphorous in CD-P-M **4** was 18% of the weight according to ICP-OES experiments, which is in agreement with the presence of 20 PO_3Na_2 groups per molecule suggesting either full phosphorylation or partial oligophosphorylation of the β -CD moiety. Several attempts to obtain an estimated molecular weight by MS techniques failed.

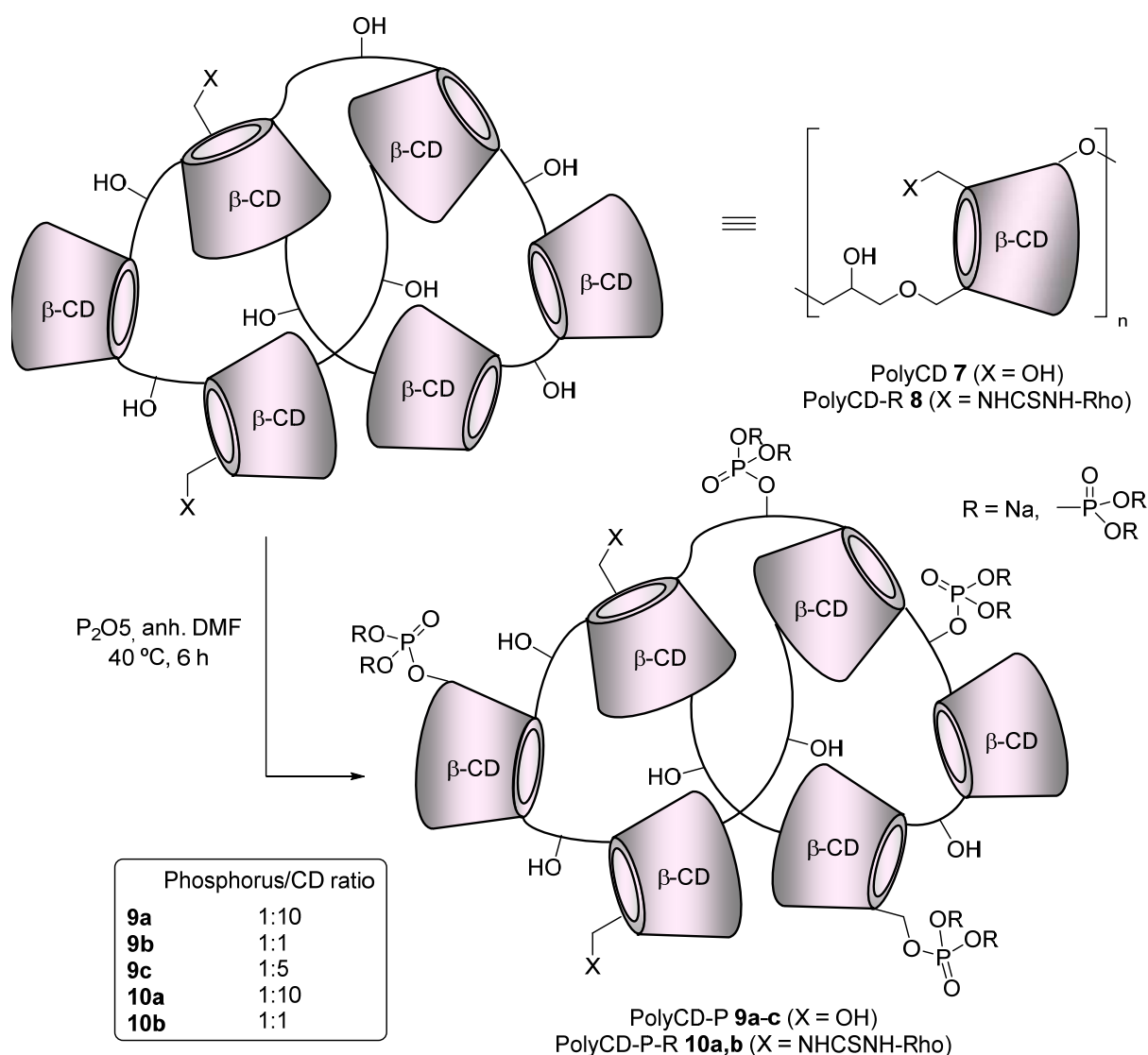
For endowing imaging properties to MIL-100(Fe) nanoMOFs, we decided to derivatize them with 6-monorhodaminylthioureido-labeled β -CD **5** (Scheme 2), a recently reported mixture of regioisomers [34]. Rhodamine B is widely used as fluorescent probe for imaging in living cells due to its desirable photophysical properties such as high molar extinction coefficients, excellent quantum yields, and tolerance to photobleaching [31,42,43,44]. Rhodamine-containing β -CD **5** was treated with P_2O_5 in DMF at 40 °C. After neutralization and dialysis, the solvent removal gave the phosphate derivative CD-P-R **6**. The phosphate groups were randomly substituted onto the hydroxyl groups of the CD. The presence of phosphate groups in CD-P-R **6** was also confirmed by ^{31}P -NMR, which showed several resonances in the range from 2.3 to -21.8 ppm.



Scheme 2. Synthesis of rhodamine β -CD phosphate sodium salt CD-P-R **6**. Phosphorylation is a random process that can take place at any hydroxylated position and may introduce both phosphate and oligophosphate groups.

In order to test the applicability of our method to more complex structures, we also partly a phosphorylated epichlorohydrin-crosslinked β -CD polymer polyCD **7** [27,35] as well as its rhodamine-labeled analogue polyCD-R **8** (Scheme 3). The use of CD-based polymers as coating materials for MOFs is expected to offer several advantages towards the monomeric

analogues such as improved shell stability and stronger interaction with the drug molecules. These benefits should allow slowing down the kinetics of drug release, the active molecules being retained longer by the coating networks, and creating a dual delivery system where different therapeutics can be loaded either within the inner or outer compartment. Phosphorylation conditions described above for the preparation of CD-P-M **4** and CD-P-R **6** were also used for the preparation of phosphorylated polymers polyCD-P **9a-c** and polyCD-P-R **10a,b** starting from polyCD **7** [27,35] and its rhodamine-labeled analogue polyCD-R **8**, respectively. Varying the amount of P_2O_5 used in the reactions, different number of phosphate groups grafted on the polyCDs could be obtained. Three phosphorylated derivatives **9a-c** from polyCD **7** were prepared using the molar ratio 1:10, 1:1 and 1:5 phosphorus atom-CD unit 1:1, respectively, for the synthesis. In the case of polyCD-P-R **8** only 1:10 and 1:1 ratios were used to achieve **10a,b**, respectively. ^{31}P -NMR measurements confirmed the presence of phosphate groups in polymers **9a-c** and **10a,b** since several resonances in the range from 4.3 to -18.8 ppm were observed on their spectra



Scheme 3. Synthesis of polyCD phosphate sodium salts **9a-c** and **10a,b**. Epichlorohydrin cross-linking can involve both primary and secondary faces of β -CD in a random fashion. In polyCD-R **8** only a number of β -CD moieties contain rhodamine (Rho) appendages [37]. Phosphorylation is a random process that can take place at any hydroxylated position, including polymer linkers, and may introduce both phosphate and oligophosphate groups.

3.2 nanoMOF coating

MIL-100(Fe) nanoMOF were successfully obtained by microwave-assisted hydrothermal reaction. Their mean diameter was 190 ± 40 nm according to DLS measurements and the BET surfaces were $1650\text{ m}^2\text{g}^{-1}$ as characterized by N_2 adsorption measurements. The features of the nanoMOFs (specific surfaces, sizes, crystallinity) were similar to those of previously described MIL-100(Fe) nanoMOF particles [38,39,45].

NanoMOFs were modified with a CD-based shell in a simple one-step method by impregnation with aqueous solution containing the corresponding phosphorylated β -CD derivative (CD-P, CD-P-M **4**, CD-P-R **6**, or polyCD-Ps **9a-c** or **10a,b**). At the end of the incubation the nanoparticles were recovered by centrifugation, washed with water in order to remove the excess of non-attached coating molecules, and characterized by DLS, N_2 adsorption, XRPD and TEM. The diameters of the nanoMOFs increased after the coating (10-25% variation) with the highest increase in the case of polymeric CDs. Only in the case of CD polymers with the highest phosphate density (1:1) aggregation occurred. The aggregates were possibly formed by a bridging effect between nanoMOFs bearing iron sites at the surface able to coordinate with a large number of phosphates on CD polymers.

Remarkably, in all cases, the amount of CD-based materials attached to the nanoMOFs reached 20-26 wt%, in agreement with previously reported data [19], and monomers or polymers were adsorbed onto the NanoMOF surfaces within less than one hour incubation. This clearly shows the strong affinity of nanoMOFs for phosphated (macro)molecules. Moreover, whatever the coating material, nanoMOF particles preserved their faceted type morphology as assessed by TEM before and after modification (Fig. 2). The crystalline porous structure was not disrupted upon CD-based material attachment, as the BET surfaces were similar before ($1650 \pm 150\text{ m}^2\text{g}^{-1}$) and after ($1570 \pm 350\text{ m}^2\text{g}^{-1}$) coating.

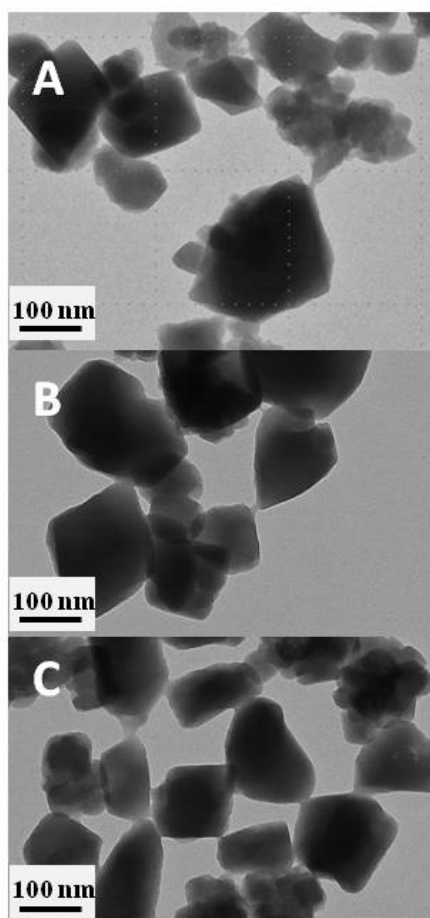


Fig. 2. Typical TEM images for unmodified nanoMOFs (A), β -CD-P coated nanoMOFs (B) and polyCD-P_{1:5} **9c** modified nanoMOFs (C).

The synthesized fluorescent CD monomers and polymers were useful to study the stability of the shells formed on the nanoMOFs under simulated biological conditions. The coating stability was investigated by spectrofluorimetry (Fig. 3). NanoMOFs were impregnated with CD-P-R **6** and polymers **10a,b** in PBS. Within the first 6 hours incubation, around 20 up to 40% of the amount of coating material was detached from the nanoMOFs, meaning that in all cases studied here, the coating represented still more than 10 % of the nanoparticles's weight.

The less phosphorylated polymer **10a** (1:10 phosphorous atom/CD unit) underwent a more substantial detachment than CD-P-R **6** bearing an average of 4 phosphate groups per CD unit, showing 62 ± 4 % and 36 ± 3 % release at 24h, respectively. On the contrary, the more substituted **10b** (1:1 phosphorus atom-CD unit) showed a better stability, comparable to that for CD-P-R **6**. It is noteworthy that when a polymeric structure is used the number of anchoring groups per CD moiety required for similar coating decreases by four times. These

results highlight the concurrence of factors others than simple cooperative effect of phosphates in the case of the CD polymers, related to the substitution degree, the spatial distribution, and the accessibility of the anchoring moieties. Both in the cases of **6** and **10b**, less than 30 % of the coating is detached in PBS after 24 hours incubation at 37°C which can be considered as satisfactory for biological applications taking into account that nanoparticles generally circulate in the blood stream in shorter time frames [19]. The stability of the shells formed on the nanoMOFs was further assessed by confocal fluorescence microscopy (Fig. 1 SI). When incubation the particles in cell culture media in the presence of 10% fetal bovine serum (FBS) for 24 h at 37 °C, the particles were still fluorescent.

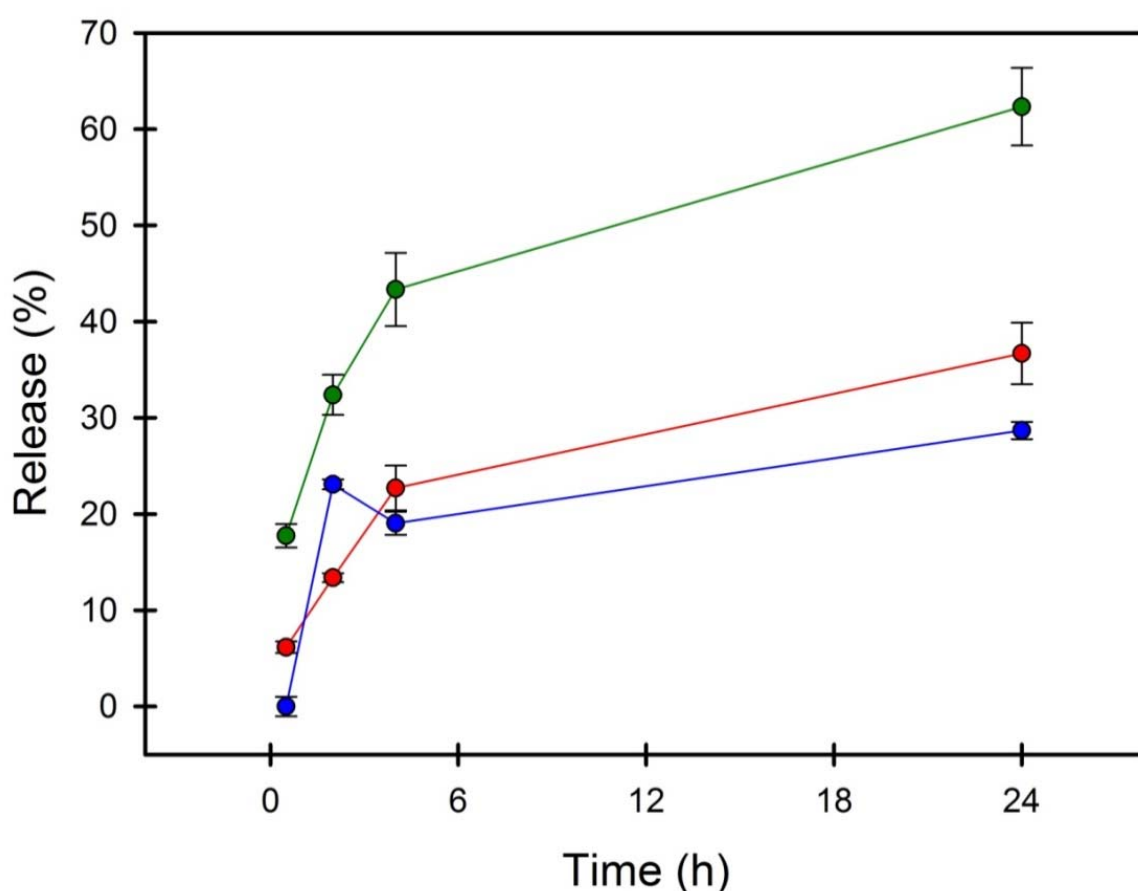


Fig. 3. Detachment of CD-P-R **6** (red) and polyCD-P-R **10a,b** (green for 1:10 and blue for 1:1) coatings during incubation in PBS at 37 °C.

3.3 Thermodynamics of interaction

The binding processes of the phosphorylated β -CD derivatives CD-P and CD-P-M **4** to the nanoMOFs surface in aqueous media were thermodynamically studied by ITC (Fig. 4).

Interestingly, this technique showed strong interactions but different thermodynamic behavior for each coating molecule. In the case of CD-P, an exothermic event was followed by an endothermic phenomenon, indicating that two different events take place during the interaction. A first hypothesis takes into consideration the possible interactions with the two types of nanoMOFs cages, the large and the small ones, since both of them might have different reactivities towards CD-P. However, taking into account that the chemical composition is the same whatever the type of cage, it seems more reasonable to presume that the observed events are due to very fast and specific interactions between the grafted phosphate groups and the iron trimers. Indeed, native β -CD without phosphate groups does not interact with the nanoMOFs (Fig. 4). It has been previously demonstrated that the phosphate-iron coordination is the principal binding mechanism of CD-P to the nanoMOFs surface [19]. Phosphate-iron coordination induces a dehydration of the cages structure, signature of the observed endothermic events. Each interacting phosphate group is able to replace one coordinated water molecule. There is one water molecule per each iron trimer, which constitutes together with trimesic acid the MOF structure. The binding isotherm for the CD-P/nanoMOF interaction was characterized by a $\Delta G \sim -37.6 \text{ kJ mol}^{-1}$ and $\Delta H \sim -62.8 \text{ kJ mol}^{-1}$ associated with an unfavorable entropic contribution ($-T\Delta S \sim 25.1 \text{ kJ mol}^{-1}$) [19]. This event is followed by the entropy driven dehydration ($\Delta H \sim 17.6 \text{ kJ mol}^{-1}$ and $-T\Delta S \sim -48.2 \text{ kJ mol}^{-1}$).

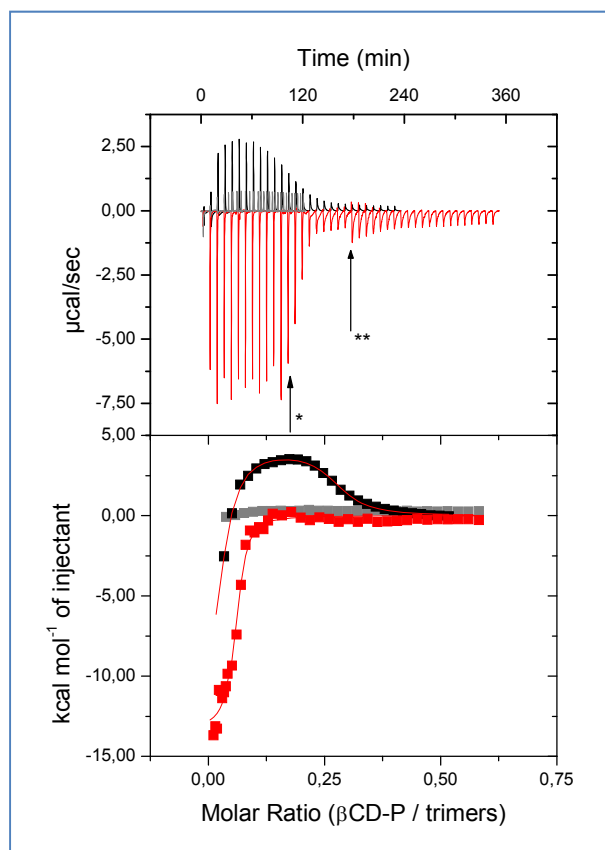


Fig. 4. ITC experiments for CD-P (2.3 mM) (black), CD-P-M **4** (5.06 mM) (red) and β -CD (5.06 mM) (grey) with MIL-100(Fe) nanoMOF (0.93 mM for CD-P; 1.9mM for **4** and β -CD). The top

panel shows raw data denoting the amount of generated heat following each injection of phosphate derivative. For CD-P-M **4**, the 10 first injections of 2 μL were followed by 10 injections of 5 μL (see *) and the last ones of 10 μL (see **). The area under each peak represents the amount of heat released/absorbed upon binding of CD-P, CD-P-M **4** to nanoMOFs. The bottom panel shows the enthalpogram, where the area was integrated and plotted against the molar ratio of CD-P or CD-P-M **4** to iron trimers.

In contrast, in the case of the interaction between CD-P-M **4** and nanoMOFs only the exothermic phenomenon was detected under the considered experimental conditions (Fig. 4). Such interaction was characterized by a prevailing favourable enthalpic contribution ($\Delta H \sim -55.7 \text{ kJ mol}^{-1}$) that overcomes the negative entropic contribution of $-\Delta S \sim 25.2 \text{ kJ.mol}^{-1}$.

Despite of the different behavior, in both cases it seems clear that the complexation of the phosphate groups with the iron trimers is an exothermic driven mechanism where the favourable enthalpic terms compensate the unfavourable entropic contributions. CD-P-M **4** bears around 20 phosphate groups, whereas CD-P has only 3 to 4 phosphate groups. These chemical composition differences could explain why in the first case, prevailing exothermic events were observed, corresponding to a plethora of possibilities of interaction between the phosphate groups and the iron trimers.

ITC measurements also indicated strong ITC binding phenomena between the phosphorylated polymers polyCD-P_{1:10} **9a** and polyCD-P_{1:5} **9c** and the nanoMOFs (Fig. 5). Interestingly, the similarity of the obtained enthalpograms for these two polymers containing different phosphate/CD ratios (1:10 and 1:5, respectively) indicates that the number of grafted phosphate groups on polyCD has little influence on the interaction with nanoMOFs. In both cases, favourable entropic major contributions as well as exothermic enthalpic terms are found. These behaviour contrasts with the previously described thermodynamics for the interaction between the monomeric form CD-P and the nanoMOFs, which exhibits a negative enthalpic contribution followed by an unfavourable entropic component. It seems clear that Interactions between polyCD bearing phosphate groups and nanoMOF surfaces are more complex than the interaction involving CD-P. Due to the crosslinked bulky structure of the water soluble CD polymers, it seems plausible that only some of the CD-grafted phosphate groups are accessible to interact with the nanoMOFs. Indeed, it has been previously shown that some CDs in the cross-linked CD polymers are not accessible because of steric hindrance [27,28,29], and this might also be the case for the grafted phosphate groups. Besides, polymers undergo conformational changes when adsorbing at interfaces and this results in additional events detected by ITC. As a consequence of polymers needing to adapt their conformation to get adsorbed after each injection in contrast to monomers, the time frame of the interactions might be longer for polymers **9a,c** than monomers CD-P and CD-P-M **4**. Thus, the observed entropic signature with polymers **9a,c** can be attributed

to the dehydration of the cages as previously discussed in the case of monomers but also from changes in polymer conformation.

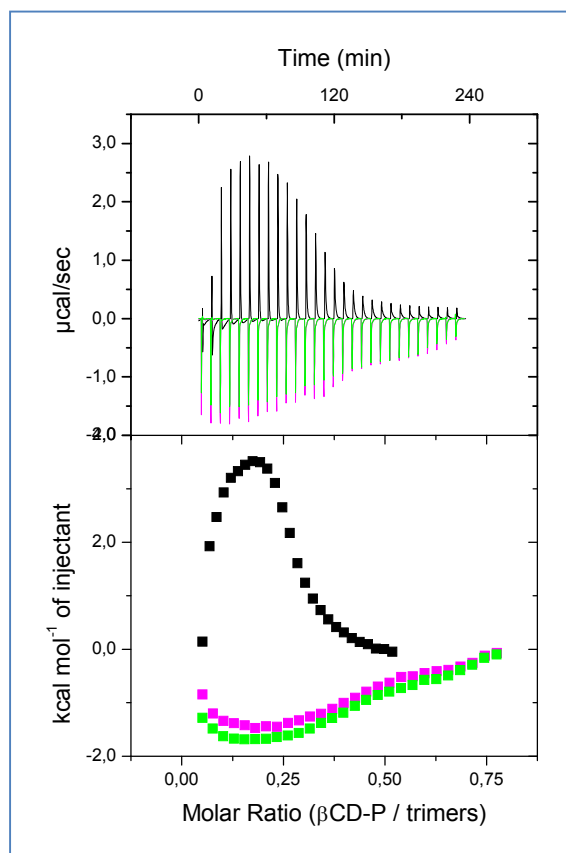


Fig. 5. ITC experiments for CD-P (2.3mM) (black), and polyCD-P_{1:10} **9a** (3.4 mM) (green) and polyCD-P_{1:5} **9c** (3.4 mM) (pink) with MIL-100(Fe) nanoMOF (0.93 mM). The top panel shows raw data denoting the amount of generated heat following each injection of phosphate derivative. The area under each peak represents the amount of heat released/absorbed upon binding of phosphate derivatives to nanoMOFs. The bottom panel shows the enthalpogram: The area was integrated and plotted against the molar ratio of CD-P or polyCD-Ps **9a,c** to iron trimers.

In a nutshell, the ITC results show a strong interaction between both phosphate monomeric and polymeric CDs with the NanoMOF, corroborating the *in vitro* shell stability results. However, significant differences in the thermodynamic profiles were observed when compared, suggesting a more complex behavior in the case of CD polymers. The presence of favourable entropic major contributions for the latter might be related with conformational changes due to an induce-fit effect which is not expected for the monomeric phosphate CD derivatives. In addition, the similarity between the interaction of the nanoMOFs with the polyCD-P_{1:5} and polyCD-P_{1:10} confirms that the functionalization degree influence is affected by the accessibility of the anchoring groups due to the steric hindrance.

For drug entrapment and release studies, the effect of monomeric CD-P shells was compared with that of polymeric CD-P shells.

3.4. Drug loading and release

The effect of CD-P, polyCD-P_{1:10} **9a** and polyCD-P_{1:5} **9c** on the stability of nanoMOFs-drug loading complexes was investigated. One of the most challenging drug candidates for encapsulation is the antiretroviral drug AZT-TP [39]. MIL-100(Fe) nanoMOFs were loaded with 8 wt% of AZT-TP by impregnation in aqueous drug solutions as previously described. Then, nanoMOFs were coated with CD-P or polyCDs **9a,b** by additional one hour impregnation in corresponding aqueous solutions. At the end of the incubation, the drug payload was practically unchanged since less than 1% of drug was lost after surface modification (Table 1).

Table1. Amount of CD-P or polyCD-Ps **9a,c** associated to the nanoparticles after 1 h of impregnation and amount of AZT-TP released during the coating process.

Sample	Amount of coating (wt%)	AZT-TP release after impregnation (%)
CD-P	20 (±3)	0.4 (±0.05)
PolyCD-P _{1:10} 9a	25.4 (±0.3)	0.1 (±0.03)
PolyCD-P _{1:5} 9c	26.4(±0.5)	0.8 (±0.5)

Drug release in PBS was progressive from all the studied nanoMOFs (Fig. 6). At the beginning of the release process, there were little differences between uncoated and polyCD coated nanoMOFs, however, after one day release, significant differences were observed.

After one day, it appears that the polymeric CD coating slows the release of the entrapped AZT-TP. For example, 82 and 83 % of the drug is released from uncoated and CD-P coated particles, respectively. This result is not surprising considering that AZT has been reported to interact with native β -CD and β -CD modified at the primary face [46,47], while CD-P is randomly phosphorylated on both sides of the macrocycle. In contrast, only 72% of the drug is released from the polyCD-coated ones after the same lapse of time, increasing drug retention in 13 %. This is possibly because the presence of a number of unmodified CD moieties in the polymeric coating that interact with the drug, slowing down its release. As demonstrated here, polymeric CD coatings are thicker than monomeric ones, offering numerous opportunities for interaction with drugs.

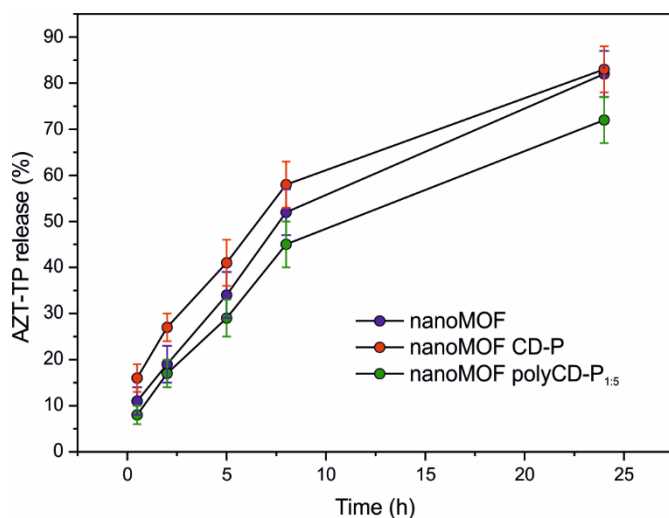


Fig. 6. AZT-TP release from uncoated and CD-P or polyCD-P_{1.5} coated nanoMOFs in PBS at 37 °C.

Taking into account these findings, it could be expected that polymeric CD shells would exert an even better control upon drug release in the case of drugs with higher affinities for CDs such as doxorubicin, camptothecin, methotrexate, 5-fluorouracil, etc [48,49]. Besides, the polymeric shells could be used as scaffolds for further grafting fluorescent dyes and/or targeting ligands.

4. Conclusion

We have synthesized a series of randomly phosphorylated β -CD derivatives bearing or not mannosylated moieties, rhodamine-containing β -CD as well as epichlorohydrin-crosslinked β -CD polymers and their rhodamine labeled analogues. Such phosphate derivatives along with commercially available β -CD phosphate sodium salt were used to coat, in a non-covalent manner, the surface of MIL-100(Fe) nanoMOFs. Surface functionalization of nanoMOFs was achieved by an easy, fast and reproducible method, assimilated to a non-covalent, efficient and convenient “click chemistry” strategy without byproducts. Results in this study show that the number of phosphate grafting moieties is not the only element involved in the anchoring event. Instead, factors such as accessibility due to steric hindrance, spatial distribution, induce-fit effects or possibility of cross-linking between several nanoparticles seem to operate simultaneously in the case of CD polymeric coatings, making difficult to predict the stability of a given β -CD polymer as a coating shell on MOFs nanoparticles as compared to monomeric analogues. Polymeric CD coatings, however, afford a better control of drug release over monomeric ones probably due to the presence of non-modified CD moieties in the structure. This study opens the way towards the preparation of

versatile drug-loaded core-shell nanoMOF particles in water, by simple self-assembling procedures.

Supplementary material

Supplementary data to this article can be found online at

Acknowledgments

The authors acknowledge the French Research Agency for support through the ANR-14-CE08-0017 grant and the Spanish Ministry of Economy and Competitiveness (Grant CTQ2013-48380-R). This research was funded by European Union through FP7-PEOPLE-2013-ITN (<http://itn-cyclonhit.eu>) project (Grant Agreement n°608407).

REFERENCES

-
- [1] B. F. Hoskins, R. Robson, Infinite polymeric frameworks consisting of three dimensionally linked rod-like segments, *J. Am. Chem. Soc.* 111 (1989) 5962-5964, doi: 10.1021/ja00197a079.
- [2] S. Kitagawa, H.-C. Zhou, Ed., Themed issue on Metal Organic Frameworks (MOFs), *Chem. Soc. Rev.* 43 (2014) 5403-6176.
- [3] V. Rodriguez-Ruiz, A. Maksimenko, R. Anand, S. Monti, V. Agostoni, P. Couvreur, M. Lampropoulou, K. Yannakopoulou, R. Gref, Efficient “green” encapsulation of a highly hydrophilic anticancer drug in metal–organic framework nanoparticles, *J. Drug Target.* 23 (2015) 759-767, doi: 10.3109/1061186x.2015.1073294.
- [4] S. Wuttke, S. Braig, T. Preiß, A. Zimpel, J. Sicklinger, C. Bellomo, J. O. Rädler, A. M. Vollmar, T. Bein, MOF nanoparticles coated by lipid bilayers and their uptake by cancer cells, *Chem. Commun.* 51 (2015) 15752-15755, doi: 10.1039/c5cc06767g.
- [5] P. Horcajada, T. Chalati, C. Serre, B. Gillet, C. Sebrie, T. Baati, J. F. Eubank, D. Heurtaux, P. Clayette, C. Kreuz, J.-S. Chang, Y. K. Hwang, V. Marsaud, P. Bories, L. Cynober, S. Gil, G. Férey, P. Couvreur, R. Gref, Porous metal-organic-framework nanoscale carriers as a potential platform for drug delivery and imaging, *Nat. Mater.* 9 (2010) 172-178, doi: 10.1038/nmat2608.
- [6] P. Horcajada, R. Gref, T. Baati, P. K. Allan, G. Maurin, P. Couvreur, G. Férey, R. E. Morris, C. Serre, Metal-organic frameworks in biomedicine, *Chem. Rev.* 112 (2012) 1232-1268, doi: 10.1021/cr200256v.
- [7] M. R. di Nunzio, V. Agostoni, B. Cohen, R. Gref, A. Douhal, A “ship in a bottle” strategy to load a hydrophilic anticancer drug in porous metal organic framework nanoparticles: efficient encapsulation, matrix stabilization, and photodelivery, *J. Med. Chem.* 57 (2014) 411–420, doi: 10.1021/jm4017202.

-
- [8] M. Giménez-Marqués, T. Hidalgo, C. Serre, P. Horcajada, Nanostructured metal–organic frameworks and their bio-related applications 307 (2016) 342-360, doi: 10.1016/j.ccr.2015.08.008.
- [9] P. P. Bag, D. Wang, Z. Chen, R. Cao, Outstanding drug loading capacity by water stable microporous MOF: a potential drug carrier, *Chem. Commun.* 52 (2016) 3669-3672, doi: 10.1039/c5cc09925k.
- [10] Q.-L. Li, J.-P. Wang, W.-C. Liu, X.-Y. Zhuang, J.-Q. Liu, G.-L. Fan, B.-H. Li, W.-N. Lin, J.-H. Man, A new (4,8)-connected topological MOF as potential drug delivery, *Inorg. Chem. Commun.* 55 (2015) 8-10, doi: 10.1016/j.inoche.2015.02.023.
- [11] C. Orellana-Tavra, E. F. Baxter, T. Tian, T. D. Bennett, N. K. H. Slater, A. K. Cheetham, D. F.-Jimenez, Amorphous metal–organic frameworks for drug delivery, *Chem. Commun.* 51 (2015) 13878-13881, doi: 10.1039/c5cc05237h.
- [12] T. Baati, L. Njim, F. Neffati, A. Kerkeni, M. Bouttemi, R. Gref, M. F. Najjar, A. Zakhama, P. Couvreur, C. Serre, P. Horcajada, In depth analysis of the in vivo toxicity of nanoparticles of porous iron(III) metal-organic frameworks, *Chem. Sci.* 4 (2013) 1597-1607, doi: 10.1039/c3sc22116d.
- [13] R. Gref, A. Domb, P. Quellec, T. Blunk, R. H. Müller, J. M. Verbavatz, R. Langer, The controlled intravenous delivery of drugs using PEG-coated sterically stabilized nanospheres, *Adv. Drug Deliv. Rev.* 16 (1995) 215-233, doi: 10.1016/0169-409x(95)00026-4.
- [14] R. A. Petros, J. M. DeSimone, Strategies in the design of nanoparticles for therapeutic applications, *Nat. Rev. Drug Discov.* 9 (2010) 615-627, doi: 10.1038/nrd2591.
- [15] M. Meldal, C. W. Tornøe, Cu-catalyzed azide-alkyne cycloaddition, *Chem. Rev.* 108 (2008) 2952-3015, doi: 10.1021/cr0783479.
- [16] C. D. Hein, X. M. Liu, D. Wang, Click chemistry, a powerful tool for pharmaceutical sciences, *Pharm. Res.* 25 (2008) 2216-2230, doi: 10.1007/s11095-008-9616-1.
- [17] E. Lallana, A. Sousa-Herves, F. Fernandez-Trillo, R. Riguera, E. Fernandez-Megia, Click chemistry for drug delivery nanosystems, *Pharm. Res.* 29 (2012) 1-34, doi: 10.1007/s11095-011-0568-5.
- [18] A. Aykaç, M. C. Martos-Maldonado, J. M. Casas-Solvas, I. Quesada-Soriano, F. García-Maroto, L. García-Fuentes, A. Vargas-Berenguel, β -Cyclodextrin-bearing gold glyconanoparticles for the development of site specific drug delivery systems, *Lagmuir* 30 (2014) 232-242, doi: 10.1021/la403454p.
- [19] V. Agostoni, P. Horcajada, M. Noiray, M. Malanga, A. Aykaç, L. Jicsinszky, A. Vargas-Berenguel, N. Semiramo, S. Daoud-Mahammed, V. Nicolas, C. Martineau, F. Taulelle, J. Vigneron, A. Etcheberry, C. Serre, R. Gref, A "green" strategy to construct non-covalent, stable and bioactive coatings on porous MOF nanoparticles, *Sci. Rep.* 5 (2015) 7925, doi: 10.1038/srep07925.
- [20] J. Szejtli, T. Osa (Vol. Eds.), *Cyclodextrins*, in: J. L. Atwood, J. E. D. Davies, J.-M. Lehn, D. D. MacNicol, F. Vögtle (Series Eds.), *Comprehensive Supramolecular Chemistry*, Pergamon, Oxford, 1996, Vol. 3.
- [21] H. Dodziuk, *Cyclodextrins and their complexes: Chemistry, analytical methods, applications*, Wiley-VCH, Weinheim, 2006.
- [22] T. Loftsson, D. Duchêne, *Cyclodextrins and their pharmaceutical applications*, *Int. J. Pharm.* 329 (2007) 1-11, doi: 10.1016/j.ijpharm.2006.10.044.

-
- [23] A. Vargas-Berenguel, F. Ortega-Caballero, J. M. Casas-Solvas, Supramolecular chemistry of carbohydrate clusters with cores having guest binding abilities, *Mini-Rev. Org. Chem.* 4 (2007) 1-14, doi: 10.2174/157019307779815901.
- [24] R. Gref, D. Duchêne, Cyclodextrins as "smart" components of polymer nanoparticles, *J. Drug Delivery Sci. Technol.* 22 (2012) 223-234, doi:10.1016/s1773-2247(12)50033-x.
- [25] G. M. Pavlov, E. V. Korneeva, N. A. Smolina, U. S. Schubert, Hydrodynamic properties of cyclodextrin molecules in dilute solutions, *Eur. Biophys. J.* 39 (2010) 371-379, doi: 10.1007/s00249-008-0394-9.
- [26] P. Horcajada, S. Surblé, C. Serre, D.-Y. Hong, Y.-K. Seo, J.-S. Chang, J.-M. Grenèche, I. Margiolaki, G. Férey, Synthesis and catalytic properties of MIL-100(Fe), an iron(III) carboxylate with large pores, *Chem. Commun.* (2007) 2820-2822, doi: 10.1039/b704325b.
- [27] S. Daoud-Mahammed, C. Ringard-Lefebvre, N. Razzouq, V. Rosilio, B. Gillet, P. Couvreur, C. Amiel, R. Gref, Spontaneous association of hydrophobized dextran and poly- β -cyclodextrin into nanoassemblies: formation and interaction with a hydrophobic drug, *J. Colloid Interface Sci.* 307 (2007) 83-93, doi:10.1016/j.jcis.2006.10.072.
- [28] S. Daoud-Mahammed, P. Couvreur, K. Bouchemal, M. Chéron, G. Lebas, C. Amiel, R. Gref, Cyclodextrin and polysaccharide-based nanogels: entrapment of two hydrophobic molecules, benzophenone and tamoxifen, *Biomacromolecules* 10 (2009) 547-554, doi: 10.1021/bm801206f.
- [29] K. Bouchemal, P. Couvreur, S. Daoud-Mahammed, J. Poupaert, R. Gref, A comprehensive study on the inclusion mechanism of benzophenone into supramolecular nanoassemblies prepared using two water-soluble associative polymers, *J. Therm. Anal. Calorim.* 98 (2009) 57-64, doi: 10.1007/s10973-009-0452-2.
- [30] D. D. Perrin, W. F. L. Armarego, *Purification of Laboratory Chemicals*, 3rd ed., Pergamon: Oxford, 1989.
- [31] A. L. Martin, B. Li, E. R. Gillies, Surface functionalization of nanomaterials with dendritic groups: Toward enhanced binding to biological targets, *J. Am. Chem. Soc.* 131 (2009) 734-741, doi: 10.1021/ja807220u.
- [32] J. M. Casas-Solvas, A. Vargas-Berenguel, Synthesis of a β -cyclodextrin derivative bearing an azobenzene group on the secondary face, *Tetrahedron Lett.* 49 (2008) 6778-6780, doi: 10.1016/j.tetlet.2008.09.032.
- [33] J. M. Casas-Solvas, E. Ortiz-Salmerón, I. Fernández, L. García-Fuentes, F. Santoyo-González, A. Vargas-Berenguel, Ferrocene- β -cyclodextrin conjugates: Synthesis, supramolecular behavior, and use as electrochemical sensors, *Chem. Eur. J.* 15 (2009) 8146-8162, doi: 10.1002/chem.200900593.
- [34] M. Malanga, L. Jicsinszky, E. Fenyvesi, Rhodamine-labeled cyclodextrin derivatives, *J. Drug Deliv. Sci. Technol.* 22 (2012) 260-265, doi:10.1016/S1773-2247(12)50037-7.
- [35] E. Renard, A. Deratani, G., Volet, B. Sébille, Preparation and characterization of water soluble high molecular weight β -cyclodextrin-epichlorohydrin polymers, *Eur. Polymer J.* 33 (1997) 49-57, doi: 10.1016/S0014-3057(96)00123-1.
- [36] R. Gref, C. Amiel, K. Molinard, S. Daoud-Mahammed, B. Sébille, B. Gillet, J.C. Beloeil, C. Ringard, V. Rosilio, J. Poupaert, P. Couvreur, New self-assembled nanogels based on host-guest interactions: characterization and drug loading, *J. Contr. Release* 111 (2006) 316-324, doi: 10.1016/j.jconrel.2005.12.025.

-
- [37] M. Malanga, M. Bálint, I. Puskás, K. Tuza, T. Sohajda, L. Jicsinszky, L. Szente, E. Fenyvesi, Synthetic strategies for the fluorescent labeling of epichlorohydrin-branched cyclodextrin polymers, *Beilstein J. Org. Chem.* 10 (2014) 3007-3018, doi:10.3762/bjoc.10.319.
- [38] V. Agostoni, P. Horcajada, V. Rodriguez-Ruiz, H. Willaime, P. Couvreur, C. Serre, R. Gref, 'Green' fluorine-free mesoporous iron(III) trimesate nanoparticles for drug delivery, *Green Mater.* 1 (2013) 209-217, doi: 10.1680/gmat.13.00001.
- [39] V. Agostoni, T. Chalati, P. Horcajada, H. Willaime, R. Anand, N. Semiramo, T. Baati, S. Hall, G. Maurin, H. Chacun, K. Bouchemal, C. Martineau, F. Taulelle, P. Couvreur, C. Rogez-Kreuz, P. Clayette, S. Monti, C. Serre, R. Gref, Towards an improved anti-HIV activity of NRTI via metal-organic frameworks nanoparticles, *Adv. Healthc. Mater.* 2 (2013) 1630-1637, doi: 10.1002/adhm.201200454.
- [40] Z. Juvancz, L. Jicsinszky, K. E. Markides, Phosphated cyclodextrins as new acidic chiral additives for capillary electrophoresis, *J. Microcolumn Sep.* 9 (1997) 581-589, doi: 10.1002/(SICI)1520-667X(1997)9:8<581::AID-MCS1>3.0.CO;2-Y.
- [41] S. Cherenok, J. Dutasta, V. Kalchenko, Phosphorus-containing chiral macrocycles, *Curr. Org. Chem.* 10 (2006) 2307-2331, doi: 10.2174/138527206778992725.
- [42] J. R. Lakowicz, *Principles of fluorescence spectroscopy*, Springer, Singapore, 2006.
- [43] L. Yuan, W. Lin, K. Zheng, L. He, W. Huang, Far-red to near infrared analyte-responsive fluorescent probes based on organic fluorophore platforms for fluorescence imaging, *Chem. Soc. Rev.* 42 (2013) 622-661, doi: 10.1039/c2cs35313j.
- [44] J. Chan, S. C. Dodani, C. J. Chang, Reaction-based small-molecule fluorescent probes for chemoselective bioimaging, *Nat. Chem.* 4 (2012) 973-984, doi: 10.1038/nchem.1500.
- [45] V. Agostoni, R. Anand, S. Monti, S. Hall, G. Maurin, P. Horcajada, C. Serre, K. Bouchemal, R. Gref, Impact of phosphorylation on the encapsulation of nucleoside analogues within porous iron(III) metal-organic framework MIL-100(Fe) nanoparticles, *J. Mater. Chem. B* (2013) 4231-4242, doi: 10.1039/c3tb20653j.
- [46] M. Sillion, A. Dascalu, B. C. Simionescu, M. Pinteala, C. Ungurenasu, Synthesis and anti-HIV activity of β -cyclodextrin-C6-sulfate/3-azido-3'-deoxythymidine inclusion complex, *J. Polym. Sci., A* 49 (2011) 1730-1733, doi: 10.1002/pola.24581.
- [47] P. Kumar, Y. E. Choonara, L. C. du Toit, V. Pillay, In silico elucidation of the inclusion phenomenon and permeation behavior of a zidovudine-cyclodextrin complex via static lattice atomistic simulation, *J. Incl. Phenom. Macrocycl. Chem.* 78 (2014) 445-455, doi: 10.1007/s10847-013-0316-z.
- [48] R. Anand, M. Malanga, I. Manet, F. Manoli, K. Tuza, A. Aykaç, C. Ladavière, E. Fenyvesi, A. Vargas-Berenguel, R. Gref, S. Monti, Citric acid- γ -cyclodextrin crosslinked oligomers as carriers for doxorubicin delivery, *Photochem. Photobiol. Sci.* 12 (2013) 1841-1854, doi: 10.1039/c3pp50169h.
- [49] B. Gidwani, A. Vyas, A Comprehensive Review on Cyclodextrin-Based Carriers for Delivery of Chemotherapeutic Cytotoxic Anticancer Drugs, *Biomed. Res. Int.* 2015 (2015) 198268, doi: 10.1155/2015/198268.